Supplement of The Cryosphere, 19, 6023–6042, 2025
https://doi.org/10.5194/tc-19-6023-2025-supplement

The Cryosphere Open Access EGU

Supplement of

Future changes in Antarctic near-surface winds: regional variability and key drivers under a high-emission scenario

Cécile Davrinche et al.

Correspondence to: Cécile Davrinche (davrinche.cecile@gmail.com)

S1 Supplementary material to "Materials and methods"

S1.1 Selection of AWS based on dataset length

To test whether datasets are long enough to be representative of a climatological period, we compute, using ERA5, the minimum value of N_{July} for which the standard error on the mean value of the July wind speed between 1980 and 2020 is inferior to 5 % of the mean value:

$$\frac{\sigma_{July}}{\sqrt{N_{July}}} < 0.05 \cdot |\overrightarrow{\overline{V_{July}}}| \quad \Rightarrow \quad N_{July} > (\frac{\sigma_{July}}{0.05 \cdot |\overrightarrow{\overline{V_{July}}}|})^2 \tag{S1}$$

With N_{july} the number of available complete July (i.e. at least 75 % of the daily values) AWS measurement series, and $|\overrightarrow{\overline{V_{July}}}|$ the mean value of July 1980-2020 wind speed in the nearest gridcell of ERA5. With that threshold, we expect to get an approximation of the mean value of the dataset which remains close to the true value of the mean over 1980-2020.

Additionally, we also decide to keep only datasets with N_{july} greater than 10. We find that this second criterion is more restrictive than the one on the relative uncertainty of the mean (Figure S1). Therefore, we kept this value of $N_{July} > 10$.

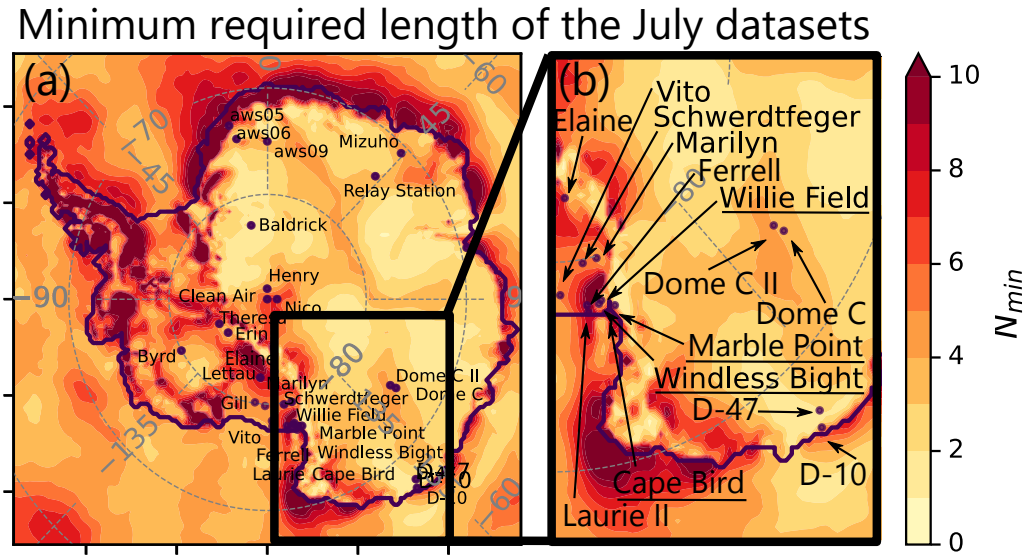

Figure S1. Maps of the minimum number of observations ($N_{min} = (\frac{\sigma_{July}}{0.05 * |\overrightarrow{\overline{V_{July}}}|})^2$), computed with ERA5 monthly output) required to evaluate the climatology of the 4 GCMs (a) over all Antarctica, (b) zoomed on the black rectangle area. Superimposed are the 28 pre-selected AWS stations for which the criterion is reached. Stations that have been discarded because of the ability of ERA5 to properly represent winds in these locations (see Sect. 2.1.4) are underlined.

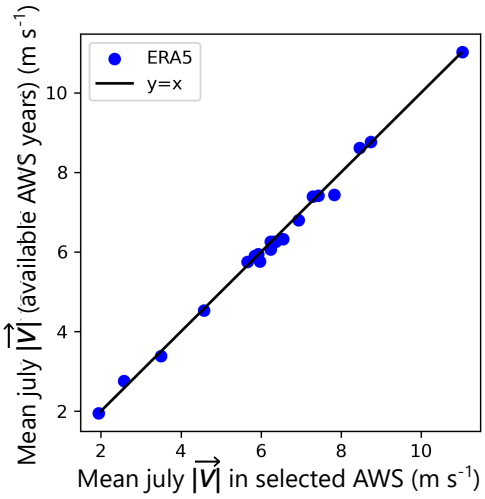

Figure S2. Comparison of ERA5 July mean values computed for all available AWS years (y axis) and for 1980-2020 (x-axis) for each of the 28 pre-selected AWS stations

S1.2 Total Performance Score

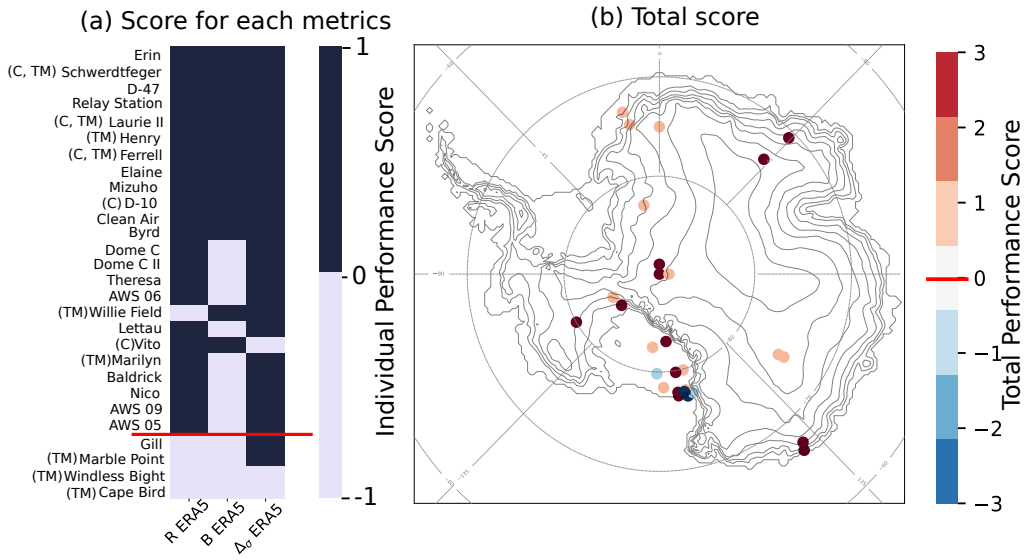

Figure S3. Score of the 28 pre-selected AWS stations compared to ERA5 for all July available AWS data Three metrics are considered: the correlation coefficient (R), the normalized mean bias (B) and the normalized standard deviation (σ_N). Each metrics for each station gives a score equal to -1 and 1 depending on its performance (see Sec. 2.1.4). Positive values indicate a good performance. (a) Scores for each metrics and for each stations. (b) Sum of all individual scores. Red solid line on the colorbar indicates the threshold value under which stations are excluded based on their comparison with ERA5. Those stations are shaded in blue.

S2 Supplementary material to: "Projected changes of the drivers of continental near-surface winds across different models"

S2.1 General changes in Antarctica

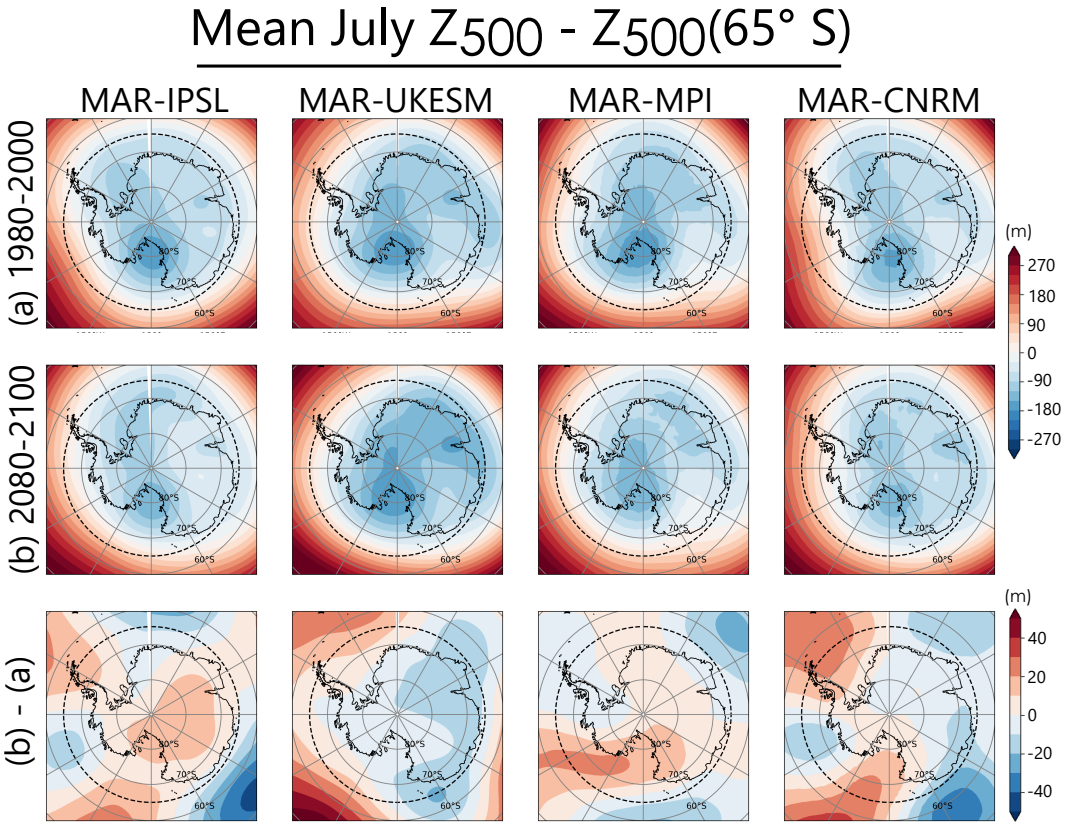

Figure S4. (a) Difference between the mean monthly July 1980-2000 geopotential height at 500 hPa and the geopotential height at 500 hPa at 65 ° S. Same as (a) but for July 2080-2100. (c) Difference of (b) and (a).

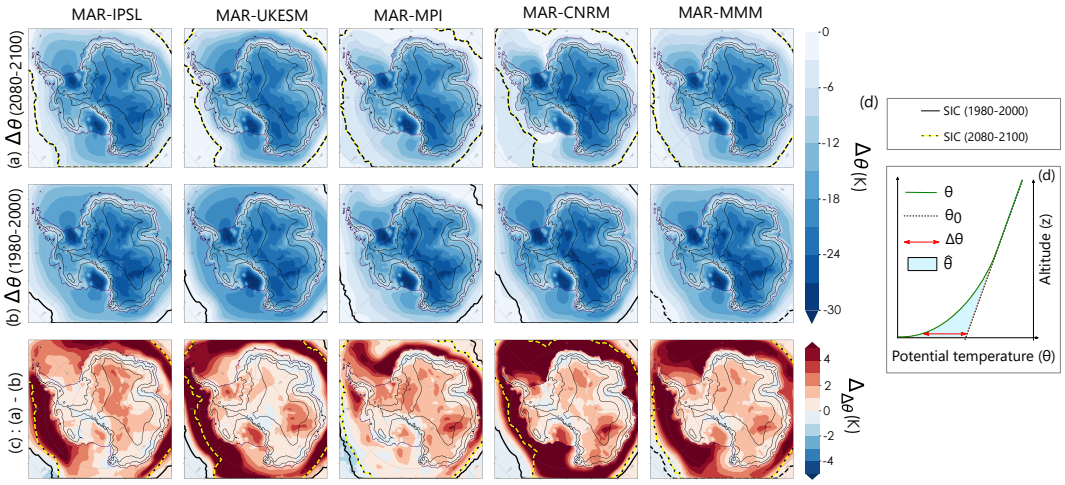

Figure S5. Changes in the strength of the July temperature inversion at 10-m ($\Delta_{\Delta\theta}$) for all models and the multi-model mean (MMM).(a) $\Delta_\theta = \theta - \theta_0$ for the historical period (1980-2000), (b) $\Delta_\theta = \theta - \theta_0$ for projections (2080-2100) and (c) changes in Δ_θ between July 2080-2100 and July 1980-2000. (d) Typical vertical profile of potential temperature and associated definition of the linear background potential temperature (θ_0), the potential temperature deficit (or inversion strength, Δ_θ) and the vertically integrated potential temperature deficit $\hat{\theta}$.

In a warming climate, due to the weaker temperature inversion layer, in coastal areas, the katabatic and thermal wind induced by horizontal changes in the depth of the temperature deficit layer decrease (FigureS7a and b). Because both forcings are acting in opposing directions, this leads to a compensation effect, especially in coastal areas. Overall, we can say that the decrease in thermal wind overcompensates for the decrease in katabatic forcing in most coastal areas (FigureS7c).

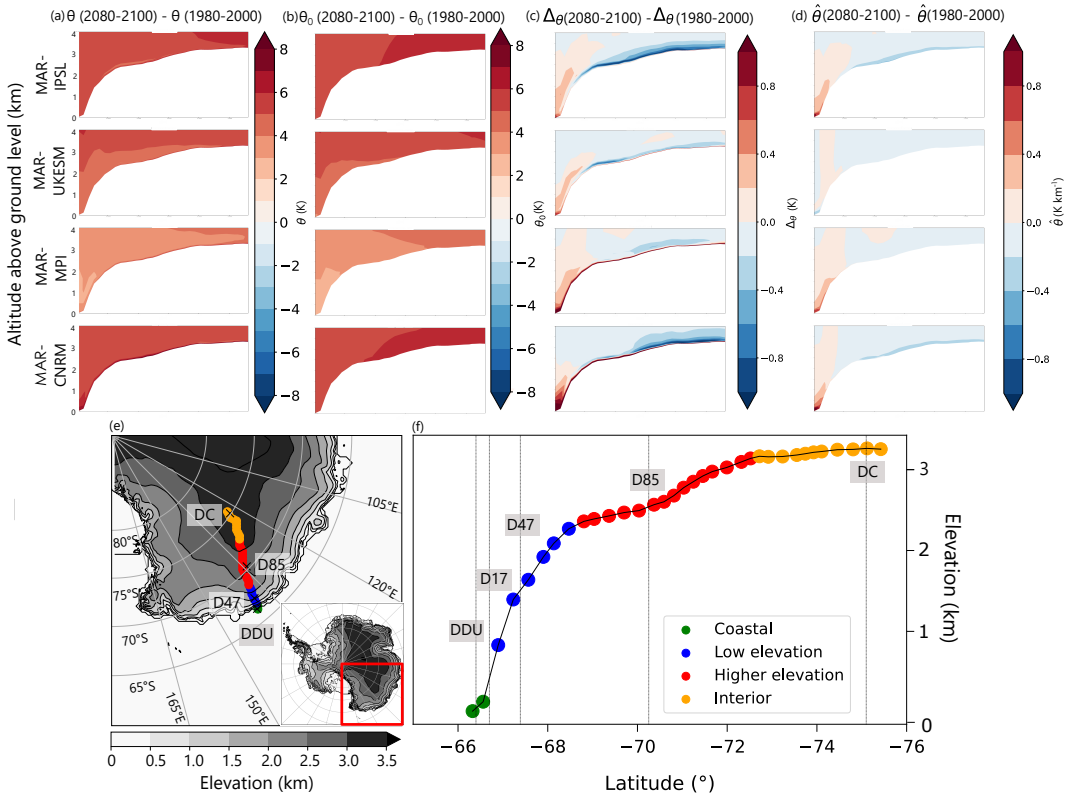

Figure S6. Changes between July 2080-2100 and July 1980-2000 on a transect running from Dumont d'Urville station to Concordia in Adélie land ((e) and (f)). Changes in (a) potential temperature (θ), (b)background potential temperature (θ_0, see Figure S5d), (c) potential temperature deficit ($\Delta\theta$, see Figure S5d) and (d) vertically integrated potential temperature deficit $\hat{\theta}$ (see Figure S5d).

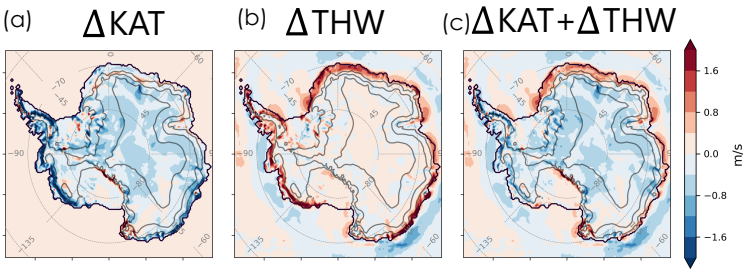

Figure S7. Projection of July 10-m changes between 2080-2100 and 1980-2000 for the multi-model mean linked to katabatic forcing (column a), thermal wind forcing (column b) and the sum of katabatic and thermal wind forcing (column c). Grey solid lines correspond to elevation contours at 0, 1000, 2000 and 3000 m.

Model	$\Delta\|\overrightarrow{V}\| > 0$	$\Delta\|\overrightarrow{V}\| > 0*$	$\Delta\|\overrightarrow{V}\| \sim 0$	$\Delta\|\overrightarrow{V}\| < 0$	$\Delta\|\overrightarrow{V}\| < 0^*$
IPSL	73%	41%	57%	27%	2%
UKESM	39%	9%	75%	61%	16%
MPI	56%	15%	75%	44%	10%
CNRM	68%	32%	68%	48%	10%
>3M	48%	8%	92%	26%	0%
MMM	65%	23%	69%	35%	8%

Table S1. Same as Table 4 but for IPSL, UKESM, MPI, CNRM (not downscaled) for at least 3 GCMs (>3M) and for the multi-GCMs mean (MMM). Underlined numbers are values for which the purcentage is higher for the ESMs than for the ESMs downscaled by MAR.

	LSC		KAT		THW + KAT	
Model	R_{ocean}	$R_{continent}$	R_{ocean}	$R_{continent}$	R_{ocean}	$R_{continent}$
MAR-IPSL	0.8	0.6	0.0	0.0	-0.2	-0.1
MAR-UKESM	0.8	0.4	0.0	0.2	-0.1	0.1
MAR-MPI	0.7	0.4	0.0	0.1	0.0	0.1
MAR-CNRM	0.7	0.3	0.0	0.1	-0.1	0.1
MAR-MMM	0.7	0.3	0.0	0.1	-0.1	0.0

Table S2. Pearson correlation coefficients between changes in wind-speed and changes in wind related to Large-scale (LSC), katabatic (KAT) and the sum of Thermal wind and katabatic (SURF = THW + KAT) on the continent and on the ocean.

S2.2 Areas of significant changes in wind speed

S2.2.1 Areas of significant increase in wind speed

For $\Delta|\overline{\vec{V}}|>0^*$

Model	ΔLSC>0*	ΔLSC<0*	ΔKAT>0*	ΔKAT<0*	ΔSURF>0*	ΔSURF<0*
MAR-IPSL	72%	0%	4%	39%	8%	40%
MAR-UKESM	71%	0%	4%	24%	2%	30%
MAR-MPI	42%	1%	4%	25%	7%	25%
MAR-CNRM	39%	3%	5%	53%	6%	46%
>3M	20%	0%	1%	33%	2%	26%
MMM	87%	1%	6%	58%	9%	52%

Table S3. For continental grid cells exhibiting a significant increase in wind speed ($\Delta|\overline{\vec{V}}|>0^*$), percentage with a significant increase in the scalar product of large scale acceleration and wind direction (ΔLSC>0*), a significant decrease in the scalar product of large scale acceleration and wind direction (ΔLSC<0*), a significant increase in the scalar product of large-scale acceleration and wind direction (ΔKAT>0*), a significant decrease in the scalar product of large-scale acceleration and wind direction (ΔKAT<0*), a significant increase in the scalar product of the sum of katabatic and thermal wind acceleration and wind direction (ΔSURF = Δ(KAT+THW)>0*), a significant decrease in the scalar product of the sum of katabatic and thermal wind acceleration and wind direction (ΔSURF = Δ(KAT+THW)<0*). Values for which changes in the scalar product of the acceleration and wind speed are greater among grid cells exhibiting a significant increase than their corresponding values among all continental grid cells are underlined.

In Enderby Land, similarly to Adélie land, there is a large area (denoted by a black and yellow dashed line on FigureS8), all models (except MAR-UKESM) agree on a significant increase in both wind speed ($\Delta|\overline{\vec{V}}| >+ 0.4$ m s^{-1} for all models) and large-scale forcing (ΔLSC $> +0.4$ m s^{-1} for all models, see Table S5 and Figure S8(a) and (b)) while changes in the surface forcing (ΔSURF, S8(c)) are weaker to negative ($-0.4 <$ ΔSURF $< +0.2$ m s^{-1} for all models, see Table S5) In this specific area, changes in wind speed appear to be related to changes in the large-scale forcing.

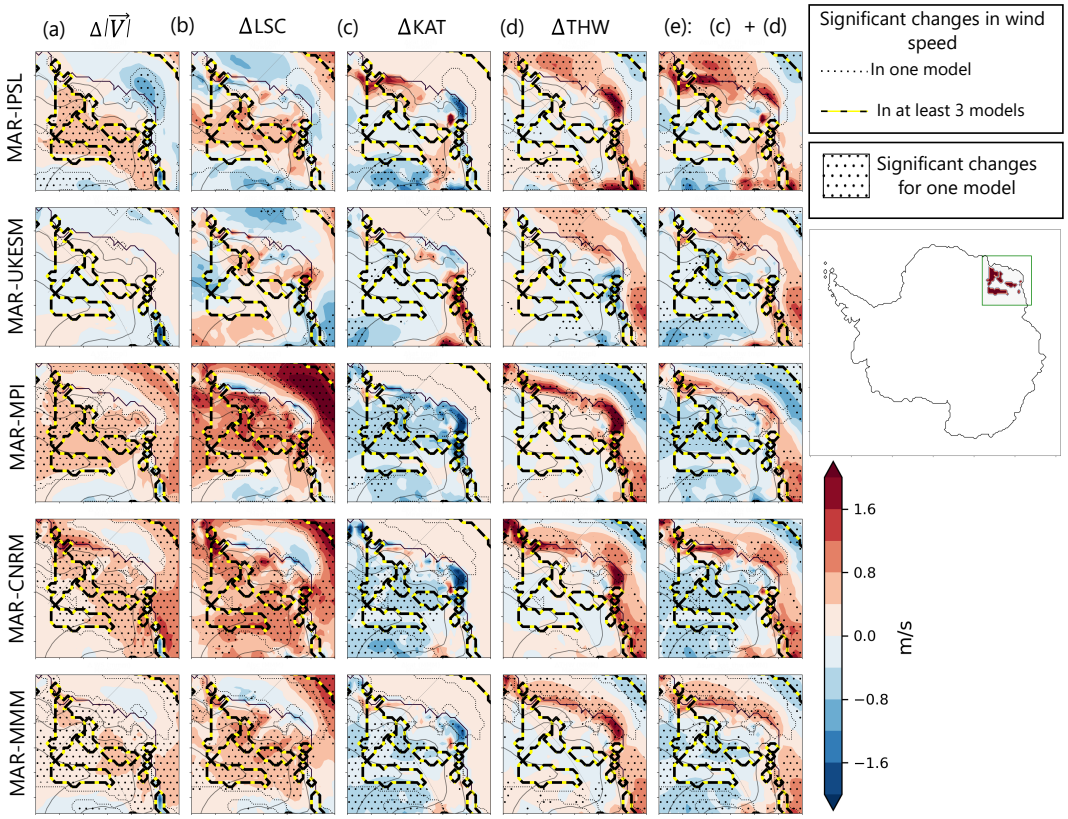

Figure S8. Same as Figure 7 in the manuscript, but for Enderby land.

S2.2.2 Tables of average changes in the forcing terms for each area of interest exhibiting a significant strengthening of wind speed

	$\Delta\|\overrightarrow{V}\|(m.s^{-1})$	$\Delta LSC(m.s^{-1})$	$\Delta SURF(m.s^{-1})$
IPSL	+0.66	+0.79	+0.36
UKESM	+0.44	+0.94	-0.18
MPI	+0.42	+0.64	-0.05
CNRM	+0.60	+0.96	-0.03
MMM	0.40	0.59	-0.04

Table S4. Mean value of the changes in wind speed ($\Delta|\overrightarrow{V}|$), scalar product of large-scale acceleration and wind direction (ΔLSC), scalar product of large-scale acceleration and accelerations due to the surface forcing ($\Delta SURF$) for grid cells exhibiting a significant increase in wind speed in Adélie Land.

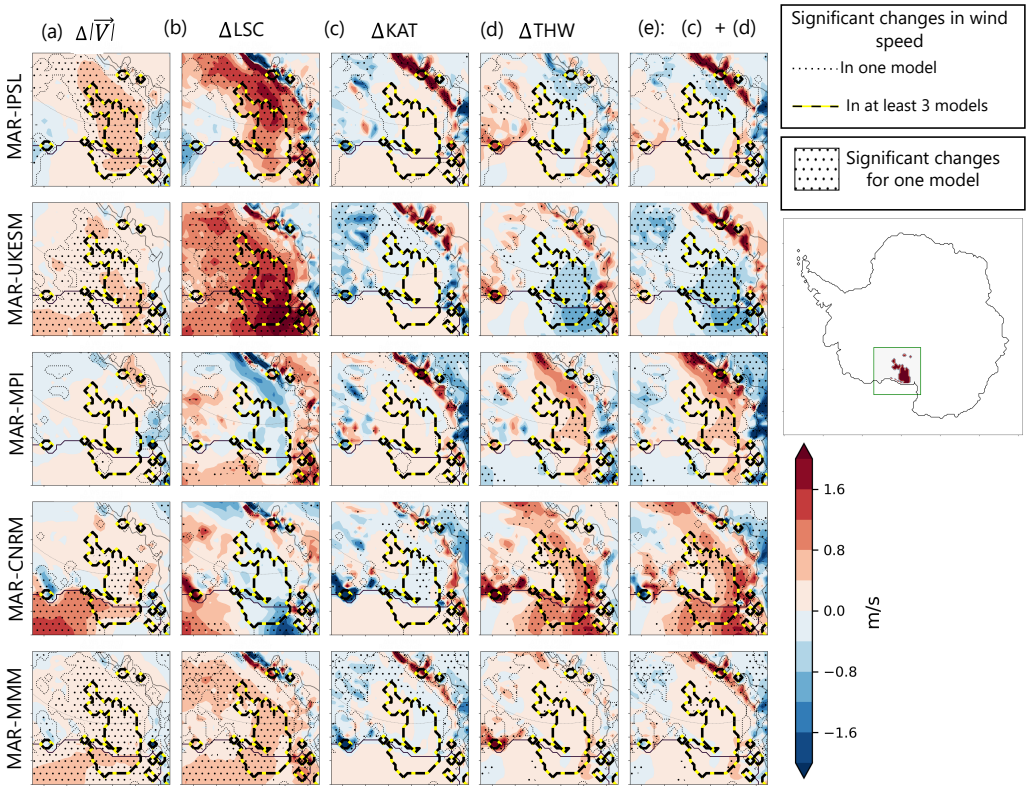

Figure S9. Same as Fig. 7 in the manuscript, but for the Ross ice shelf.

	$\Delta\|\overrightarrow{V}\|(m.s^{-1})$	$\Delta LSC(m.s^{-1})$	$\Delta SURF(m.s^{-1})$
IPSL	+0.54	+0.44	+0.12
UKESM	+0.26	+0.57	+0.18
MPI	+0.47	+0.89	-0.38
CNRM	+0.52	+0.78	-0.14
MMM	+0.33	+0.50	-0.14

Table S5. Mean value of the changes in wind speed ($\Delta|\overrightarrow{V}|$), scalar product of large-scale acceleration and wind direction (ΔLSC), scalar product of large-scale acceleration and accelerations due to the surface forcing ($\Delta SURF$) for grid cells exhibiting a significant increase in wind speed in Enderby land.

	$\Delta\|\overrightarrow{V}\|(m.s^{-1})$	$\Delta LSC(m.s^{-1})$	$\Delta SURF(m.s^{-1})$
IPSL	+0.44	+0.95	-0.04
UKESM	+0.37	+1.19	-0.29
MPI	+0.55	-0.05	+0.30
CNRM	+0.67	-0.02	+0.54
MMM	0.25	0.38	0.13

Table S6. Mean value of the changes in wind speed ($\Delta|\overrightarrow{V}|$), scalar product of large-scale acceleration and wind direction (ΔLSC), scalar product of large-scale acceleration and accelerations due to the surface forcing ($\Delta SURF$) for grid cells exhibiting a significant increase in wind speed on Ross ice-shelf.

S2.2.3 Areas of significant decrease in wind speed

Table S7. For continental grid cells exhibiting a significant decrease in wind speed ($\Delta|\overrightarrow{V}|$<0*), percentage with a significant increase in the scalar product of large scale acceleration and wind direction (ΔLSC>0*), a significant decrease in the scalar product of large scale acceleration and wind direction (ΔLSC<0*), a significant increase in the scalar product of large-scale acceleration and wind speed (ΔKAT>0*), a significant decrease in the scalar product of large-scale acceleration and wind speed (ΔKAT<0*), a significant increase in the scalar product of the sum of katabatic and thermal wind acceleration and wind speed (ΔSURF = Δ(KAT+THW)>0*), a significant decrease in the scalar product of the sum of katabatic and thermal wind acceleration and wind speed (ΔSURF = Δ(KAT+THW)<0*). Values for which changes in the scalar product of the acceleration and wind speed are greater among grid cells exhibiting a significant decrease than their corresponding values among all continental grid cells are underlined.

For $\Delta|\overrightarrow{V}|$<0*

Model	ΔLSC>0*	ΔLSC<0*	ΔKAT>0*	ΔKAT<0*	ΔSURF>0*	ΔSURF<0*
MAR-IPSL	8%	13%	4%	35%	12%	20%
MAR-UKESM	5%	11%	4%	46%	7%	33%
MAR-MPI	12%	3%	7%	50%	8%	41%
MAR-CNRM	20%	9%	3%	60%	10%	47%
>3M	3%	0%	1%	35%	4%	26%
MMM	20%	17%	4%	65%	12%	57%

On Filchner ice-shelf, similarly to Shackleton ice-shelf, there is a large area (denoted by a black and yellow dashed line on Figure S11), where all models (except MAR-IPSL) agree on a significant decrease in both wind speed ($\Delta|\overrightarrow{V}|$<- 0.4 m s^{-1} for all models) and surface forcing (ΔSURF < -0.4 m s^{-1} for all models, see TableS10 and Figure S11(a) and (b)) while changes in the large-scale forcing are weaker to positive (-0.3 < ΔSURF < +0.1 m s^{-1} for all models). In this specific area, changes in wind speed appear to be related to changes in the surface forcing.

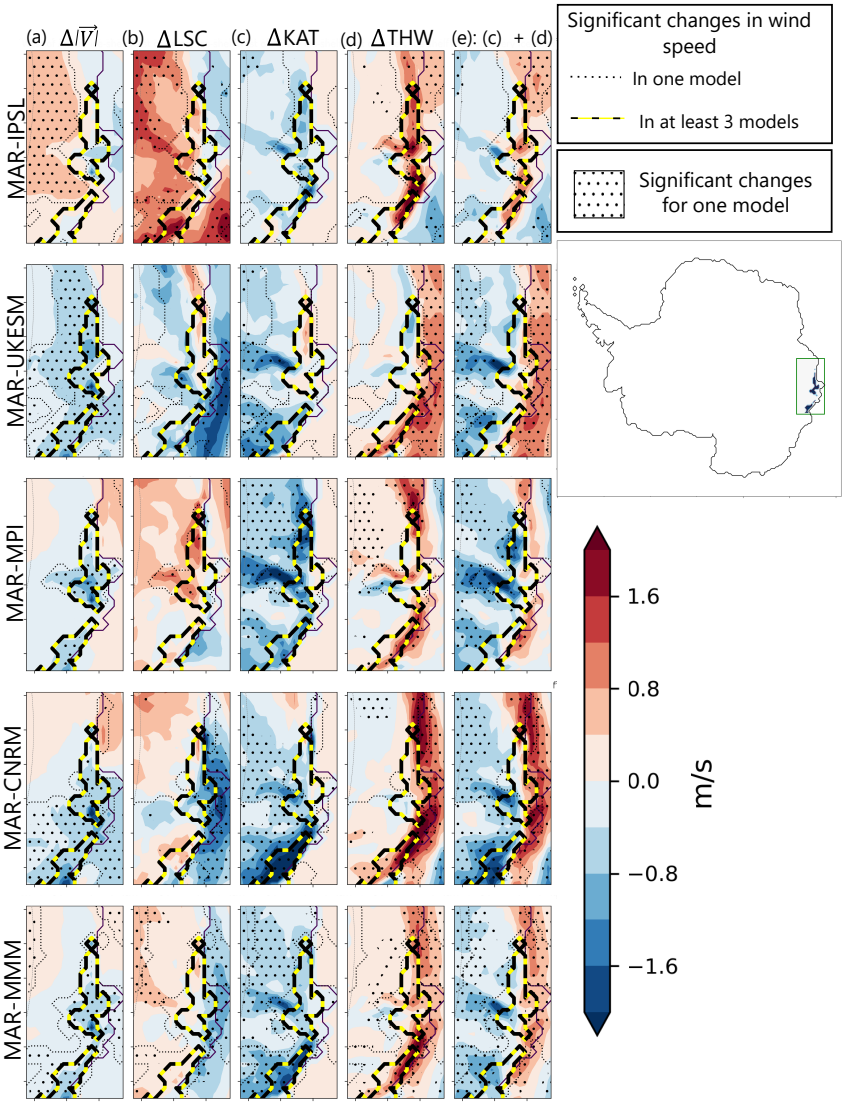

Figure S10. Same as Fig. 7 in the manuscript, but for Shackleton ice shelf.

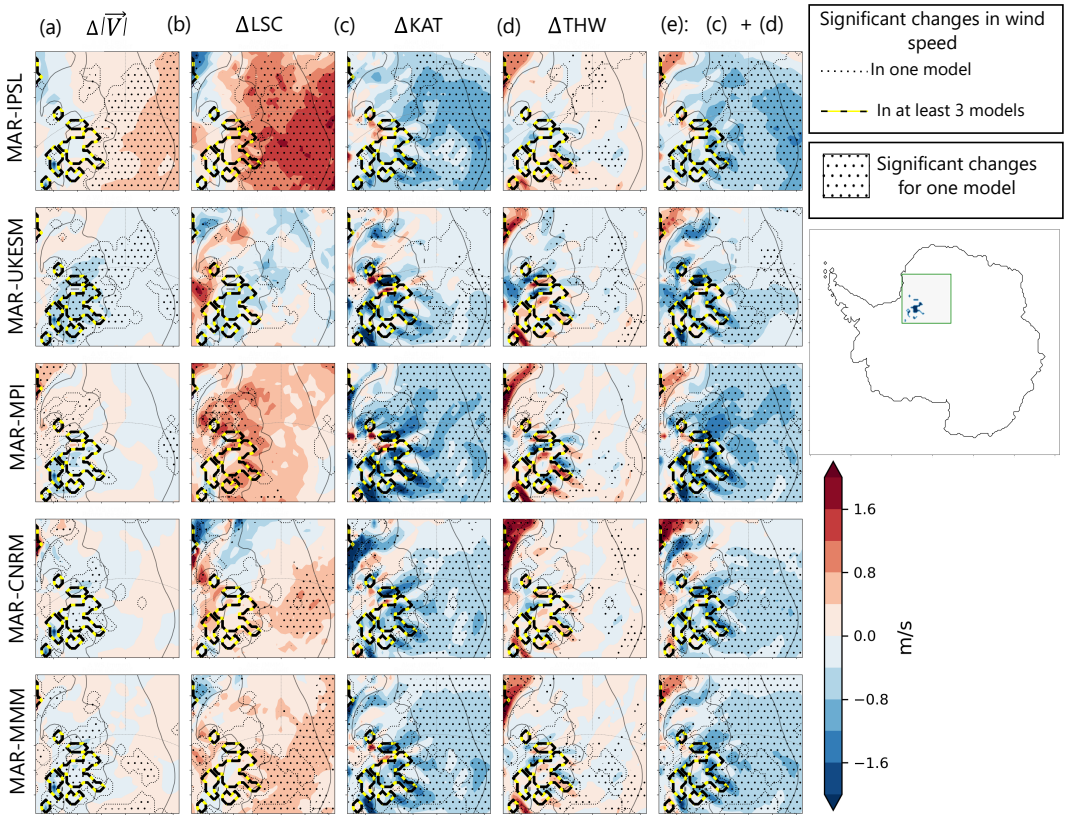

Figure S11. Same as Figure 7 in the manuscript but for Filchner ice shelf.

S2.2.4 Tables of average changes in the forcing terms for each area of interest exhibiting a significant weakening of wind speed

	$(\Delta\|\overrightarrow{V}\|(m.s^{-1})$	$\Delta LSC(m.s^{-1})$	$\Delta SURF(m.s^{-1})$
IPSL	-0.53	+0.74	-0.43
UKESM	-0.63	+0.28	-0.47
MPI	-0.77	-0.25	-0.37
CNRM	-0.71	+0.32	-0.50
MMM	-0.37	+0.40	-0.37

Table S8. Mean value of the changes in wind speed ($\Delta|\overrightarrow{V}|$), scalar product of large-scale acceleration and wind speed (ΔLSC), scalar product of large-scale acceleration and accelerations due to the surface forcing ($\Delta SURF$) for continental grid cells exhibiting a significant decrease in wind speed in the Amundsen embayment region.

	$(\Delta\|\overline{\vec{V}}\|(m.s^{-1})$	$\Delta LSC(m.s^{-1})$	$\Delta SURF(m.s^{-1})$
MAR-IPSL	-0.72	-0.02	+0.57
MAR-UKESM	-0.57	-0.34	-0.51
MAR-MPI	-0.63	+0.52	-0.80
MAR-CNRM	-0.56	-0.18	-0.47
MMM	-0.42	-0.01	-0.33

Table S9. Mean value of the changes in wind speed ($\Delta|\overline{\vec{V}}|$), scalar product of large-scale acceleration and wind speed (ΔLSC), scalar product of large-scale acceleration and accelerations due to the surface forcing ($\Delta SURF$) for continental grid cells exhibiting a significant decrease in wind speed on Shackleton ice-shelf.

	$(\Delta\|\overline{\vec{V}}\|(m.s^{-1})$	$\Delta LSC(m.s^{-1})$	$\Delta SURF(m.s^{-1})$
MAR-IPSL	-0.82	-0.21	-0.24
MAR-UKESM	-0.40	-0.25	-0.47
MAR-MPI	-0.41	+0.31	-0.96
MAR-CNRM	-0.37	+0.07	-0.44
MMM	-0.30	+0.11	-0.58

Table S10. Mean value of the changes in wind speed ($\Delta|\overline{\vec{V}}|$), scalar product of large-scale acceleration and wind speed (ΔLSC), scalar product of large-scale acceleration and accelerations due to the surface forcing ($\Delta SURF$) for continental grid cells exhibiting a significant decrease in wind speed on Filchner ice-shelf.